Determination of an additive time- and space-dependent coefficient in the heat equation

M.J. Huntul[1,2], D. Lesnic[1] and B.T. Johansson[3]
[1]*Department of Applied Mathematics, University of Leeds, Leeds LS2 9JT, UK*
[2]*Department of Mathematics, College of Science, Jazan University, Jazan, Saudia Arabia*
[3]*ITN, Campus Norrkoping, Linkoping University, Sweden*
E-mails: mmmjmh@leeds.ac.uk (M.J. Huntul), amt5ld@maths.leeds.ac.uk (D. Lesnic), tomas.johansson@liu.se (B.T. Johansson).

Abstract

Purpose - The purpose of this paper is to provide an insight and to solve numerically the identification of an unknown coefficient of radiation/absorption/perfusion appearing in the heat equation from additional temperature measurements.

Design/methodology/approach - First, the uniqueness of solution of the inverse coefficient problem is briefly discussed in a particular case. However, the problem is still ill-posed since small errors in the input data cause large errors in the output solution. For the numerical discretisation, the finite difference method combined with a regularized nonlinear minimization is performed using the MATLAB toolbox routine *lsqnonlin*.

Finding - Numerical results presented for three examples show the efficiency of the computational method and the accuracy and stability of the numerical solution even in the presence of noise in the input data.

Research limitations/implications - The mathematical formulation is restricted to identify coefficients which separate additively in unknown components dependent individually on time and space, and this may be considered as a research limitation. However, there is no research implication to overcome this since the known input data is also limited to single measurements of temperature at a particular time and space location.

Practical implications - Since noisy data are inverted, the study models real situations in which practical measurements are inherently contaminated with noise.

Social implications - The identification of the additive time- and space-dependent perfusion coefficient will be of great interest to the bio-heat transfer community and applications.

Originality/value - The current investigation advances previous studies which assumed that the coefficient multiplying the lower order temperature term depends on time or space separately. The knowledge of this physical property coefficient is very important in biomedical engineering for understanding the heat transfer in biological tissues. The originality lies in the insight gained by performing for the first time numerical simulations of inversion to find the coefficient additively dependent on time and space in the heat equation from noisy measurements.

Keywords: Inverse problem; nonlinear optimization; regularization; heat equation.

1 Introduction

Inverse problems for the parabolic heat equation consisting of determining the unknown radiative/absorption/perfusion coefficient depending on both time and space have recently received some attention, (Deng *et al.*, 2008, 2010; Savateev, 1995). The knowledge of this physical property is important in understanding the heat transfer in biological tissue, (Trucu, 2009). Its direct measurement is not available in the general case when it depends on both space and time. However, it can be inferred by inverse methods based on the measurement of the interior temperature, as considered in (Trucu *et al.*, 2011). On the other hand, this formulation means that infinitely many intrusive temperature measurements with thermocouples embedded inside the material are necessary at all space points and for all times. A possible alternative to this general inverse modelling is to restrict the generality of the coefficient by seeking it as a sum of a function dependent of time and one dependent of space. This additive class in which the admissible coefficient is sought allows to formulate an inverse problem for which measurement of the temperature in time at a single fixed space point together with measurement in space at a fixed time are sufficient to ensure that the identification is possible. A similar approach has previously been investigated in related problems concerned with the identification of an additive heat source, (Hazanee and Lesnic, 2013; Hao *et al.*, 2014). However, the inverse heat source problem is linear whilst the coefficient identification problem investigated in this paper is nonlinear and this significantly complicates its study.

The paper is structured as follows: In Section 2, the mathematical formulation of the inverse problem is given. In Section 3, the numerical solution of the direct problem based on the finite difference method (FDM) with a Crank-Nicolson scheme is briefly introduced. In Section 4, the numerical approach to solve the inverse problem based on a minimization algorithm is given. Numerical results are presented and discussed in Section 5. Finally, conclusions are stated in Section 6.

2 Mathematical formulation

Fix the parameters $L > 0$ and $T > 0$ representing the length of a finite slab and the time duration, respectively. Denote by $Q_T = \{(x, t)|\ 0 < x < L, 0 < t < T\}$ the solution domain. We consider the parabolic heat equation

$$\frac{\partial u}{\partial t}(x, t) = \frac{\partial^2 u}{\partial x^2}(x, t) + (f(t) + g(x))u(x, t), \qquad (x, t) \in Q_T, \tag{1}$$

where $f(t)$ and $g(x)$ are coefficient functions to be identified together with the temperature $u(x, t)$. In (1), the term $q(x, t) := f(t) + g(x)$ represents a radiative or perfusion coefficient. Previous studies, e.g. (Trucu *et al.*, 2008, 2010), considered the cases $g = 0$ or $f = 0$, so in that respect, our identification of an additive coefficient $q(x, t) = f(t) + g(x)$ with unknown functions f and g, is a generalization. At the other extreme, when $q(x, t)$ does not separate its identification requires the measurment of $u(x, t)$ at all points inside the solution domain Q_T, (Deng *et al.*, 2008, 2010; Trucu *et al.*, 2011), which may be impractical.

Equation (1) has to be solved subject to the initial condition

$$u(x, 0) = \phi(x), \qquad\qquad 0 \le x \le L, \tag{2}$$

the homogeneous Neumann boundary conditions

$$\frac{\partial u}{\partial x}(0,t) = \frac{\partial u}{\partial x}(L,t) = 0, \qquad\qquad 0 \le t \le T, \tag{3}$$

and the additional temperature measurements

$$u(X_0, t) = \beta(t), \qquad\qquad 0 \le t \le T, \tag{4}$$

at a fixed space location $0 < X_0 < L$, and

$$u(x, T) = \psi(x), \qquad\qquad 0 \le x \le L, \tag{5}$$

at the final time $t = T$. The conditions (3) express that the ends $\{0, L\}$ of the finite slab $(0, L)$ are insulated. In order to avoid non-uniqueness reproduced by the trivial identity $f(t) + g(x) = (f(t) + c) + (g(x) - c)$, where c is an arbitrary non-zero constant, we take a fixing condition, say at $x = X_1$ fixed in $(0, L)$, assuming that

$$g(X_1) = \alpha \tag{6}$$

is given. Alternatively, one could have a fixing condition on f instead of (6). In the above equations, the functions ϕ, β, ψ and the constant α are given, whilst the triplet of functions $f(t), g(x)$ and $u(x, t)$ are unknown. Further, assume that the conditions (2)–(5) are compatible, i.e.

$$\phi'(0) = \phi'(L) = \psi'(0) = \psi'(L) = 0, \quad \beta(0) = \phi(X_0), \quad \beta(T) = \psi(X_0). \tag{7}$$

The existence and uniqueness of a classical solution to the inverse problem (1)–(7) were established in (Savateev, 1995). Without going into too much detail, for illustration it is useful to state the unique solvability of the inverse problem (1)–(7) in a particular case, as follows.

Proposition 1. *Suppose*

$$0 < \phi \in C^4[0, L], \quad 0 < \psi \in C^4[0, L], \quad 0 < \beta \in C^1[0, T] \tag{8}$$

and assume that

$$\psi(x) = c\phi(x), \ x \in [0, L], \tag{9}$$

where $c = \beta(T)/\beta(0)$. Then the inverse problem (1)-(7) has a unique solution $(u, f, g) \in (C^2(Q_T) \cap C^1(\overline{Q_T})) \times C^1[0, T] \times C^1[0, L]$ which is explicitly given by

$$u(x, t) = \frac{\beta(t)}{\beta(0)}\phi(x), \quad (x, t) \in \overline{Q_T}, \tag{10}$$

$$f(t) = \frac{\beta'(t)}{\beta(t)} - \alpha - \frac{\phi''(X_1)}{\phi(X_1)}, \quad t \in [0, T], \tag{11}$$

$$g(x) = -\frac{\phi''(x)}{\phi(x)} + \alpha + \frac{\phi''(X_1)}{\phi(X_1)}, \quad x \in [0, L]. \tag{12}$$

Proof. We proceed as in (Savateev, 1995) and remark that from (1)–(3) using the maximum principle for the parabolic heat equation we have that $u > 0$ in $\overline{Q_T}$ and let us put

$$u = e^v. \tag{13}$$

Then equations (1)–(5) become

$$v_t(x,t) = v_{xx}(x,t) + v_x^2(x,t) + f(t) + g(x), \quad (x,t) \in Q_T, \tag{14}$$

$$v(x,0) = \ln(\phi(x)) =: \Phi(x), \quad x \in [0,L], \tag{15}$$

$$v_x(0,t) = v_x(L,t) = 0, \quad t \in [0,T], \tag{16}$$

$$v(x,T) = \ln(\psi(x)) =: \Psi(x), \quad x \in [0,L], \tag{17}$$

$$v(X_0,t) = \ln(\beta(t)) =: \beta_1(t), \quad t \in [0,T]. \tag{18}$$

From (9), (15) and (17) one can see that

$$\Psi(x) = \Phi(x) + \ln(c), \quad x \in [0,L]. \tag{19}$$

Differentiating equation (14) with respect to x we get

$$v_{tx}(x,t) = v_{xxx}(x,t) + 2v_x(x,t)v_{xx}(x,t) + g'(x), \quad (x,t) \in Q_T. \tag{20}$$

Now differentiating (20) with respect to t and using (17) we obtain, (Savateev, 1995),

$$w_t(x,t) = w_{xx}(x,t) + 2\Big(\int_T^t w(x,\tau)d\tau + \Psi'(x) \Big) w_x$$
$$+ 2\Big(\int_T^t w_x(x,\tau)d\tau + \Psi''(x) \Big) w(x,t), \quad (x,t) \in Q_T, \tag{21}$$

where

$$w(x,t) = v_{tx}(x,t). \tag{22}$$

Also, from (15)–(17), (19) and (20) one can derive that

$$w(0,t) = w(L,t) = 0, \quad t \in [0,T], \tag{23}$$

$$w(x,T) - w(x,0) = v_{xxx}(x,T) + 2v_x(x,T)v_{xx}(x,T) + g'(x) - v_{xxx}(x,0)$$
$$-2v_x(x,0)v_{xx}(x,0) - g'(x) = \Psi'''(x) + 2\Psi'(x)\Psi''(x) - \Phi'''(x) - 2\Phi'(x)\Phi''(x) = 0,$$
$$x \in [0,L]. \tag{24}$$

Then, one can observe that the initial boundary value problem for the parabolic equation (21) has only the trivial solution $w \equiv 0$. Hence, from (22) we obtain

$$v(x,t) = a(t) + b(x). \tag{25}$$

4

Then, (14)–(19) give

$$a'(t) = b''(x) + b'^2(x) + f(t) + g(x), \quad (x,t) \in Q_T, \tag{26}$$

$$\Phi(x) = \ln(\phi(x)) = a(0) + b(x), \quad x \in [0, L], \tag{27}$$

$$b'(0) = b'(L) = 0, \tag{28}$$

$$\Phi(x) + \ln(c) = \Psi(x) = \ln(\psi(x)) = a(T) + b(x), \quad x \in [0, L], \tag{29}$$

$$\beta_1(t) = \ln(\beta(t)) = a(t) + b(X_0), \quad t \in [0, T]. \tag{30}$$

From (26), we immediately obtain that

$$f(t) = a'(t) - C, \quad g(x) = -b'^2(x) - b''(x) + C, \tag{31}$$

where C is some arbitrary constant. From (27), (29) and (30) we get

$$b(x) = \ln(\phi(x)) + const., \quad a(t) = \ln(\beta(t)) + const. \tag{32}$$

Then, using (13), (25) and (32) we have

$$u(x, t) = C_1 \beta(t) \phi(x) \tag{33}$$

for some constant C_1,

$$f(t) = \frac{\beta'(t)}{\beta} - C, \quad g(x) = -\frac{\phi''(x)}{\phi(x)} + C. \tag{34}$$

Imposing (6) we obtain $C = \frac{\phi''(X_1)}{\phi(X_1)} + \alpha$ from which (11) and (12) follows. Finally, from (4), (7) and (33) we obtain that $C_1 = 1/\beta(0)$ from which (10) follows. This completes the proof of the proposition.

This proposition is useful because it indicates how to construct analytical solutions of the inverse problem (1)–(7) for which numerical methods can be assessed, see later on Examples 1 and 2 in Section 5. In addition, the explicit formulas (11) and (12) contain derivatives of the measured data which is numerically unstable. That is, although the inverse problem (1)–(7) is uniquely solvable it is still ill-posed since small errors in the input measured data (4) and (5) cause large error in the output solution for f and g. Therefore, in the numerical computation the main focus is on the development of stable nonlinear optimization algorithms, (Samarskii and Vabishchevich, 2007), as will be described in Section 4. But before we do that, in the next section we briefly describe the FDM employed for discretising the direct problem.

3   Numerical solution of the direct problem

In this section, we consider the direct initial boundary value problem given by equations (1)–(3) when f and g are given. We use the finite-difference method (FDM) with a Crank-Nicholson scheme, (Smith, 1985), which is unconditionally stable and second-order accurate in space and time. Other interesting time-stepping schemes are described in (Wood and Lewis, 1975; Lewis *et al.*, 1978). The discrete form of the direct problem is as follows. We denote $u(x_i, t_j) = u_{i,j}, f(t_j) = f_j$ and $g(x_i) = g_i$, where $x_i = i\Delta x, t_j = j\Delta t$ for $i = \overline{0, M}, j = \overline{0, N}$, and $\Delta x = \frac{L}{M}, \ \Delta t = \frac{T}{N}$.

Considering the general partial differential equation

$$u_t = G(x, t, u, u_{xx}), \tag{35}$$

the Crank-Nicolson method, (Smith, 1985), discretises (35), (2) and (3) as

$$\frac{u_{i,j+1} - u_{i,j}}{\Delta t} = \frac{1}{2}(G_{i,j} + G_{i,j+1}), \quad i = \overline{1, (M-1)}, \ j = \overline{0, (N-1)}, \tag{36}$$

$$u_{i,0} = \phi(x_i), \quad i = \overline{0, M}, \tag{37}$$

$$\frac{u_{1,j} - u_{-1,j}}{2(\Delta x)} = \frac{u_{M+1,j} - u_{M-1,j}}{2(\Delta x)} = 0, \quad j = \overline{1, N}, \tag{38}$$

where

$$G_{i,j} = G\Big(x_i, t_j, u_{i,j}, \frac{u_{i+1,j} - 2u_{i,j} + u_{i-1,j}}{(\Delta x)^2}\Big),$$

$$G_{i,j+1} = G\Big(x_i, t_{j+1}, u_{i,j+1}, \frac{u_{i+1,j+1} - 2u_{i,j+1} + u_{i-1,j+1}}{(\Delta x)^2}\Big),$$

$$i = \overline{0, M}, \quad j = \overline{0, (N-1)} \tag{39}$$

and $u_{-1,j}$ and $u_{M+1,j}$ for $j = \overline{1, N}$ are fictitious values at points located outside the computational domain.

For our problem, equation (1) is of the form (35) and the above discretisation then renders the following discrete form of (1):

$$-Au_{i-1,j+1} + (1 + B_{i,j+1})u_{i,j+1} - Au_{i+1,j+1} = Au_{i-1,j} + (1 - B_{i,j})u_{i,j} + Au_{i+1,j}, \tag{40}$$

for $i = \overline{0, M}, \ j = \overline{0, (N-1)}$, where $A = \dfrac{(\Delta t)}{2(\Delta x)^2}, \ B_{i,j} = \dfrac{(\Delta t)}{(\Delta x)^2} - \dfrac{(\Delta t)}{2}(f_j + g_i)$.

At each time step t_{j+1}, for $j = \overline{0, (N-1)}$, using the homogeneous Neumann boundary conditions (38), the above difference equation can be reformulated as an $M \times M$ system of linear equations of the form,

$$L\mathbf{u_{j+1}} = E\mathbf{u_j}, \tag{41}$$

where

$$\mathbf{u_{j+1}} = (u_{0,j+1}, u_{1,j+1}, ..., u_{M,j+1})^{\mathrm{T}},$$

$$
L = \begin{pmatrix}
1 + B_{0,j+1} & -2A & 0 & \dots & 0 & 0 & 0 \\
-A & 1 + B_{1,j+1} & -A & \dots & 0 & 0 & 0 \\
\vdots & \vdots & \vdots & \ddots & \vdots & \vdots & \vdots \\
0 & 0 & 0 & \dots & -A & 1 + B_{M-1,j+1} & -A \\
0 & 0 & 0 & \dots & 0 & -2A & 1 + B_{M,j+1}
\end{pmatrix},
$$

and

$$
E = \begin{pmatrix}
1 - B_{0,j} & 2A & 0 & \dots & 0 & 0 & 0 \\
A & 1 - B_{1,j} & A & \dots & 0 & 0 & 0 \\
\vdots & \vdots & \vdots & \ddots & \vdots & \vdots & \vdots \\
0 & 0 & 0 & \dots & A & 1 - B_{M-1,j} & A \\
0 & 0 & 0 & \dots & 0 & 2A & 1 - B_{M,j}
\end{pmatrix}.
$$

The grid convergence of the above FDM is considered next for solving the direct Neumann problem (1)–(3) with $T = L = 1$, and input data

$$
\phi(x) = u(x,0) = x^2(x-1)^2 + 1, \tag{42}
$$

$$
f(t) = \frac{1}{1+t}, \quad g(x) = \frac{-2 + 12x - 12x^2}{1 + x^2 - 2x^3 + x^4}. \tag{43}
$$

The analytical solution for the temperature is given by

$$
u(x,t) = \left(x^2(x-1)^2 + 1 \right)(1 + t). \tag{44}
$$

Figure 1 shows the surface plots of the analytical solution (44) in comparison with the numerical FDM solutions obtained with various $M = N \in \{10, 20, 40\}$. The absolute errors between those solutions are also included and it can be seen that these errors decrease as the FDM grid becomes finer.
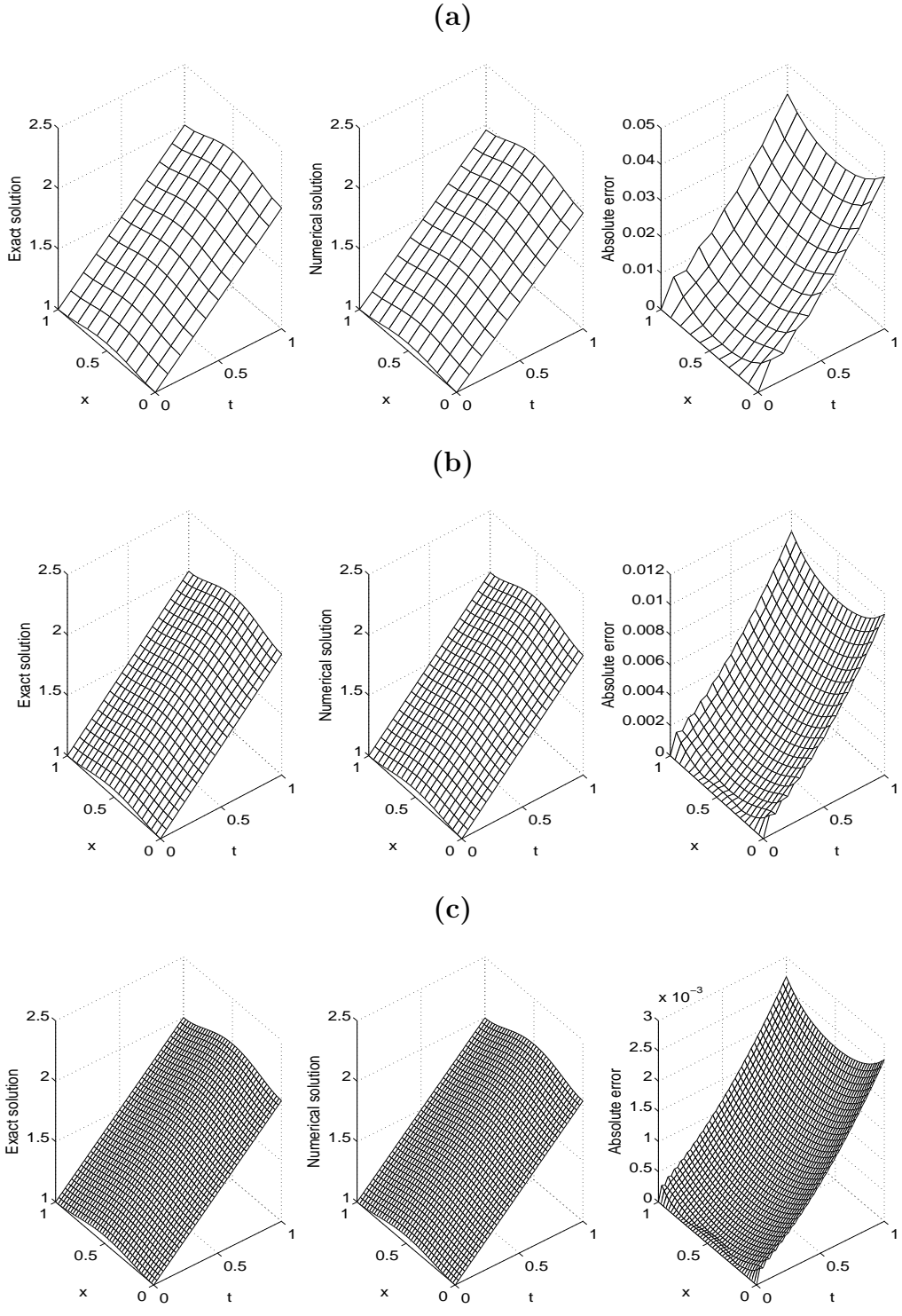
(a)

(b)

(c)

Figure 1: The exact (44) and numerical solutions for the temperature $u(x,t)$, with various mesh sizes (a) $M = N = 10$, (b) $M = N = 20$, and (c) $M = N = 40$, for the direct problem. The absolute error between them is also included.

The numerical solutions for the interior temperatures (4) and (5) are compared in

Figure 2 with the exact solutions given by

$$\beta(t) = u(X_0, t) = \frac{17}{16}(1 + t), \quad \psi(x) = u(x, T) = 2\Big(x^2(x-1)^2 + 1\Big),$$
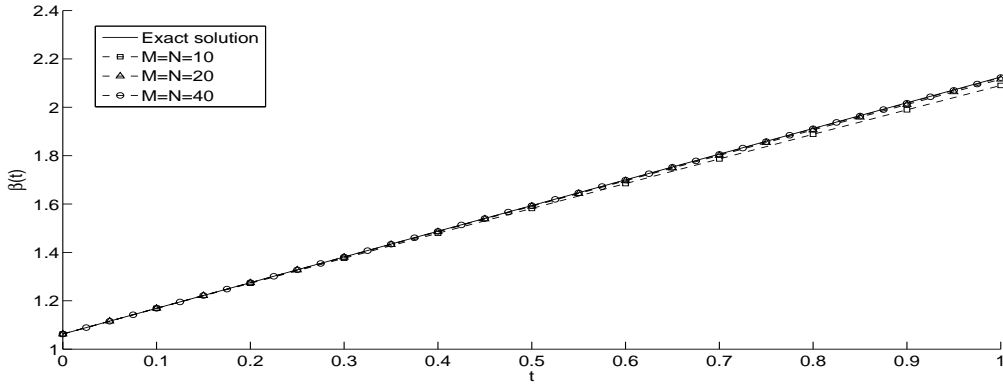
$$T = 1, \quad X_0 = \frac{1}{2}. \tag{45}$$

From Figure 2 it can be seen that the numerical solutions converge to the corresponding exact solutions (45), as the FDM grid becomes finer. In fact, the root mean square errors (rmse) defined by

$$rmse(\beta) = \sqrt{\frac{1}{N} \sum_{j=1}^{N} \Big(\beta^{numerical}(t_j) - \beta^{exact}(t_j)\Big)^2}, \tag{46}$$

$$rmse(\psi) = \sqrt{\frac{1}{M} \sum_{i=1}^{M} \Big(\psi^{numerical}(x_i) - \psi^{exact}(x_i)\Big)^2}, \tag{47}$$

indicated in Table 1, show more clearly their decreases as the grid size becomes smaller.
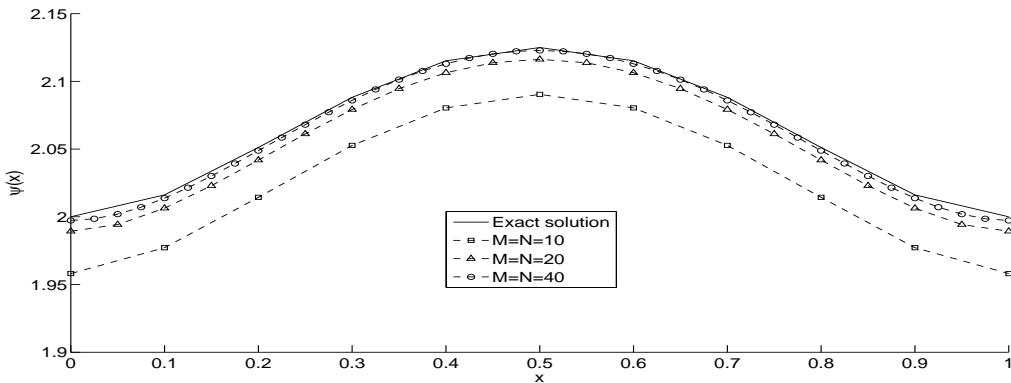
(a)

(b)

Figure 2: The exact and numerical solutions for: (a) $\beta(t)$ and (b) $\psi(x)$, various mesh sizes $M = N \in \{10, 20, 40\}$, for the direct problem.

Table 1: The $(rmse)$ given by equations (46) and (47) for $\beta(t)$ and $\psi(x)$, with various mesh sizes $M = N \in \{10, 20, 40\}$, for the direct problem.

$M = N$	10	20	40
$rmse(\beta)$	0.0179	0.0044	0.0011
$rmse(\psi)$	0.0374	0.0094	0.0024

4   Numerical approach to solve the inverse problem

In this section, we wish to obtain simultaneously the unknown functions $f(t)$ and $g(x)$ in the inverse problem (1)–(7) reformulated as minimizing the regularized objective function

$$\mathbb{F}(f, g) = \|u(x, T) - \psi(x)\|^2 + \|u(X_0, t) - \beta(t)\|^2 + \beta_1 \|f(t)\|^2 + \beta_2 \|g(x)\|^2 \\ + (g(X_1) - \alpha)^2, \tag{48}$$

where u solves (1)–(3) for given f and g, $\beta_1 \geq 0$ and $\beta_2 \geq 0$ are regularization parameters, and the norm is usually the L^2-norm. Assuming, for convenience, that we take $X_0 \in (0, L)$ such that there exists $i_0 \in \{1, ..., M\}$ for which $X_0 = x_{i_0}$, in discrete form (48) becomes

$$\mathbb{F}(\mathbf{f}, \mathbf{g}) = \frac{L}{M} \sum_{\substack{i=1 \\ i \neq i_0}}^{M} \left[u(x_i, T) - \psi(x_i) \right]^2 + \frac{T}{N} \sum_{j=1}^{N} \left[u(X_0, t_j) - \beta(t_j) \right]^2 + (g(X_1) - \alpha)^2 \\ + \beta_1 \sum_{j=1}^{N} f_j^2 + \beta_2 \sum_{i=1}^{M} g_i^2. \tag{49}$$

The value for $i = i_0$ in the first sum has been excluded in order to avoid duplicating the compatibility condition (in (7)) $u(X_0, T) = u(x_{i_0}, T) = \beta(T) = \beta(t_N) = \psi(x_{i_0}) = \psi(X_0)$.

The minimization of (49) is performed using the MATLAB toolbox routine *lsqnonlin*, which does not require the user to supply the gradient of the objective function, (Mathworks, 2012). This routine attempts to find the minimum of a sum of squares by starting from arbitrary initial guesses $\mathbf{f}^{(0)}, \mathbf{g}^{(0)}$ for $\mathbf{f}, \mathbf{g}$, respectively. We have compiled this routine with the following parameters:

- Algorithm = Trust-Region-Reflective (TRR), (Coleman and Li, 1996).

- Maximum number of iterations, (MaxIter) = 400.

- Maximum number of objective function evaluations, (MaxFunEvals) $= 10^2 \times$ (number of variables.)

- Termination tolerance on the function value, (TolFun) $= 10^{-20}$.

- x Tolerance, (xTol) $= 10^{-20}$.

- The lower and upper simple bounds are -10^3 and 10^3 for $\mathbf{f}$ and $\mathbf{g}$.

The inverse problem under investigation is solved subject to both exact and noisy data which are numerically simulated as

$$\beta^{\epsilon 1}(t_j) = \beta(t_j) + \epsilon 1_j, \quad j = \overline{1, N}, \tag{50}$$

$$\psi^{\epsilon 2}(x_i) = \psi(x_i) + \epsilon 2_i, \quad i = \overline{1, M}, \quad i \neq i_0, \tag{51}$$

where $\epsilon 1_j$ and $\epsilon 2_i$ are random variables generated from Gaussian normal distributions with mean zero and standard deviations $\sigma 1$ and $\sigma 2$ given by

$$\sigma 1 = p \times \max_{t \in [0,T]} |\beta(t)|, \quad \sigma 2 = p \times \max_{x \in [0,L]} |\psi(x)|, \tag{52}$$

where p represents the percentage of noise. We use the MATLAB function $normrnd$ to generate the random variables $\underline{\epsilon 1} = (\epsilon 1_j)_{j=\overline{1,N}}$ and $\underline{\epsilon 2} = (\epsilon 2_i)_{i=\overline{1,(M-1)}}$ given by

$$\underline{\epsilon 1} = normrnd(0, \sigma 1, N), \quad \underline{\epsilon 2} = normrnd(0, \sigma 2, M - 1). \tag{53}$$

5 Numerical results and discussion

In this section, we present examples in order to test the accuracy and stability of the numerical methods introduced in Sections 3 and 4, respectively. The root mean square errors (rmse) are used to evaluate the accuracy of the numerical results and are defined by

$$rmse(f) = \sqrt{\frac{1}{N} \sum_{j=1}^{N} \left(f^{numerical}(t_j) - f^{exact}(t_j) \right)^2}, \tag{54}$$

$$rmse(g) = \sqrt{\frac{1}{M} \sum_{i=1}^{M} \left(g^{numerical}(x_i) - g^{exact}(x_i) \right)^2}. \tag{55}$$

In all examples we take, for simplicity, $T = 1$, $L = 1$ and $X_0 = X_1 = L/2 = 0.5$. Consequently, $i_0 = M/2$ in (49). In all the inverse calculations we take $M = N = 40$.

5.1 Example 1

We solve the inverse problem (1)–(7) with unknown coefficients $f(t)$ and $g(x)$ and the input data (42), (45) and $\alpha = g(0.5) = 16/17$. From this data one can observe that the conditions of Proposition 1 of Section 2 are satisfied and hence the inverse problem has a unique solution given by (10)–(12) which yield the expressions (43) and (44). We take the inital guess as

$$f^0(t) = 1 - \frac{t}{2}, \quad g^0(x) = \begin{cases} -2 + \frac{100}{17}x, & 0 \leq x \leq 0.5, \\ \frac{66}{17} - \frac{100}{17}x, & 0.5 < x \leq 1, \end{cases} \tag{56}$$

which are straight lines passing through $f(0) = 1$, $f(1) = 1/2$, and $g(0) = -2$, $g(0.5) = 16/17$, $g(1) = -2$.

Considering no noise in the measurement data (4) and (5), the unregularized objective function (49), i.e. $\beta_1 = \beta_2 = 0$, as a function of a number of iterations plotted in Figure 3,

shows a rapid decrease to a low value of $O(10^{-29})$ in 19 iterations. Figure 4 shows the exact and numerical solutions of the functions $f(t)$ and $g(x)$, respectively. From this figure it can be seen that very accurate numerical solutions are obtained.
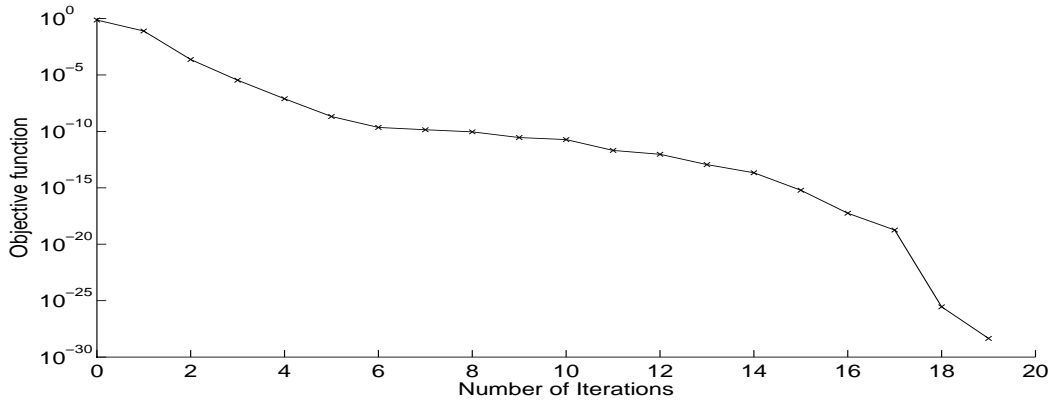

Figure 3: Objective function (49) for Example 1 with no noise and no regularization.

Next, we add a small amount of $p = 0.01\%$ noise to the measured data (4) and (5). For higher amounts of noise the numerical results were less accurate and therefore they are not presented. The point to stress here is that since the inverse problem is ill-posed then we expect that regularization is needed in order to achieve stable and accurate results. The monotonic decreasing convergence of the objective function (49), as a function of the number of iterations, is shown in Figure 5 with and without regularization. Figure 6 shows the graphs of the recovered functions. From Figure 6 it can be seen that, as expected, when $\beta_1 = \beta_2 = 0$ we obtain unstable and inaccurate solutions because the problem is ill-posed and very sensitive to noise. Thus regularization is needed in order to stabilise the solutions. We selected by trial and error the regularization parameters $\beta_1 = 10^{-9}$ and $\beta_2 = 10^{-7}$ which give stable and reasonable accurate solutions for the functions $f(t)$ and $g(x)$. For more elaborate choices of multiple regularization parameters, see (Belge et $al.$, 2002; Fornasier et $al.$, 2014).

The related numerical results for the temperature $u(x,t)$ with $p = 0.01\%$ noise, and with and without regularization, are presented in Figure 7 showing good agreement with the exact solution (44).

Other details about the number of iterations, the number of function evaluations, the value of the objective function (49) at the final iteration, the $rmse(f)$ and $rmse(g)$ in (54) and (55), respectively, and the computational time are given in Table 2. Overall, from this table as well as from Figures 3-7 it can be seen that accurate and stable numerical results are rapidly achieved by the MATLAB toolbox iterative routine $lsqnonlin$ minimizing the objective function (49).
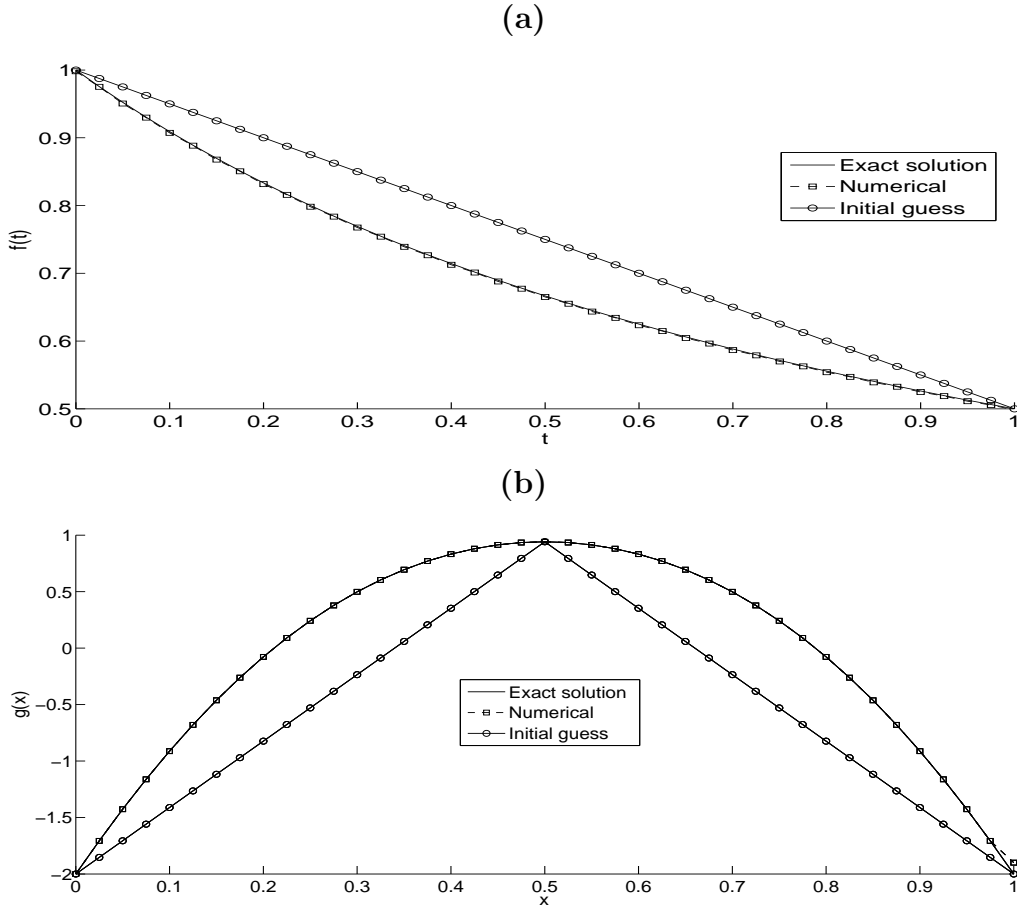
12

Figure 4: (a) Coefficient $f(t)$ and (b) coefficient $g(x)$, for Example 1 with no noise and no regularization.

Table 2: Number of iterations, number of function evaluations, value of the objective function (49) at final iteration, $rmse(f)$ and $rmse(g)$, and computational time, for Example 1.

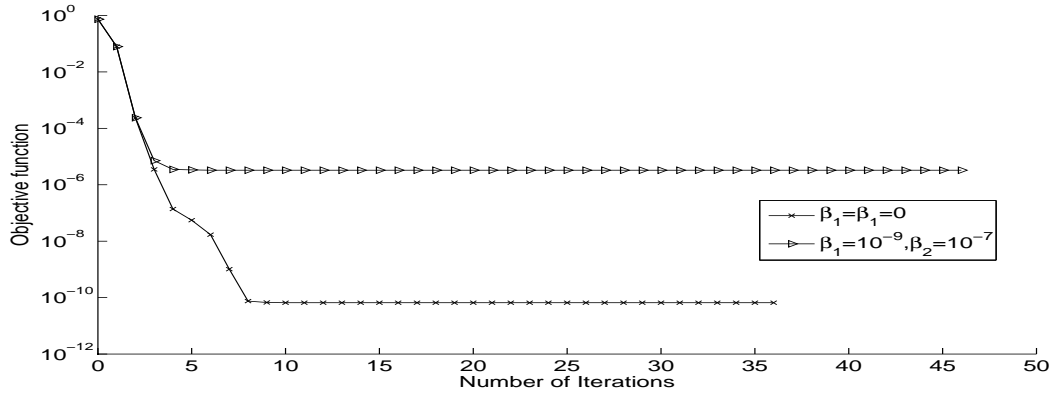| Numerical outputs	$p = 0$ $(\beta_1 = \beta_2 = 0)$	$p = 0.01\%$ $(\beta_1 = \beta_2 = 0)$	$p = 0.01\%$ $(\beta_1 = 10^{-9}, \beta_2 = 10^{-7})$
Number of iterations	19	36	46
Number of function evaluations	1660	3071	3901
Value of objective function (49) at final iteration	4.4E-29	6.5E-11	3.2E-6
$rmse(f)$	0.0013	0.1454	0.1024
$rmse(g)$	0.0156	0.6698	0.1634
Computational time (sec)	163	306	386

Figure 5: Objective function (49), for Example 1 with $p = 0.01\%$ noise, with and without regularization.
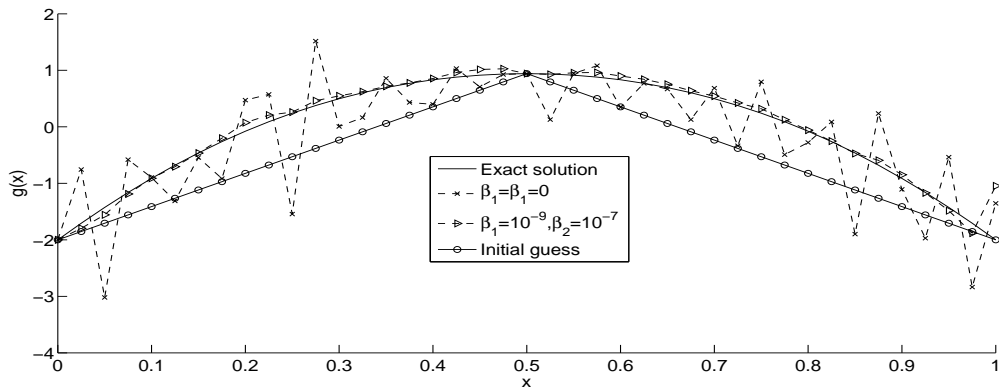
(a)
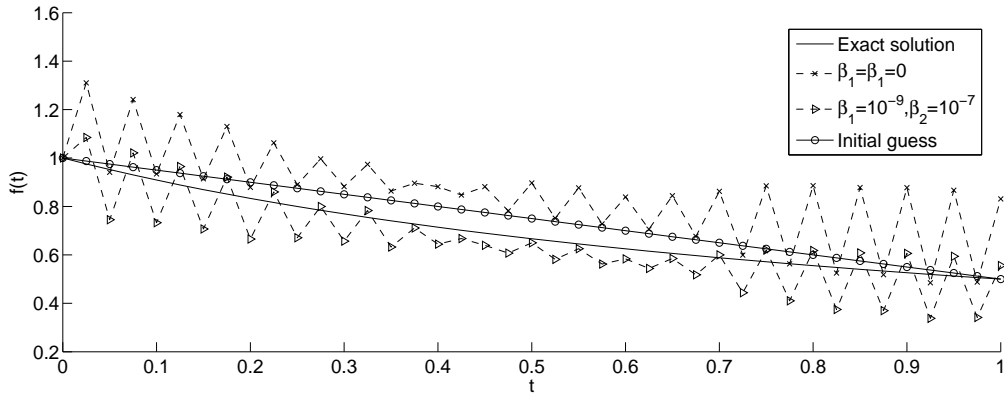
(b)

Figure 6: (a) Coefficient $f(t)$ and (b) coefficient $g(x)$, for Example 1 with $p = 0.01\%$ noise, with and without regularization.
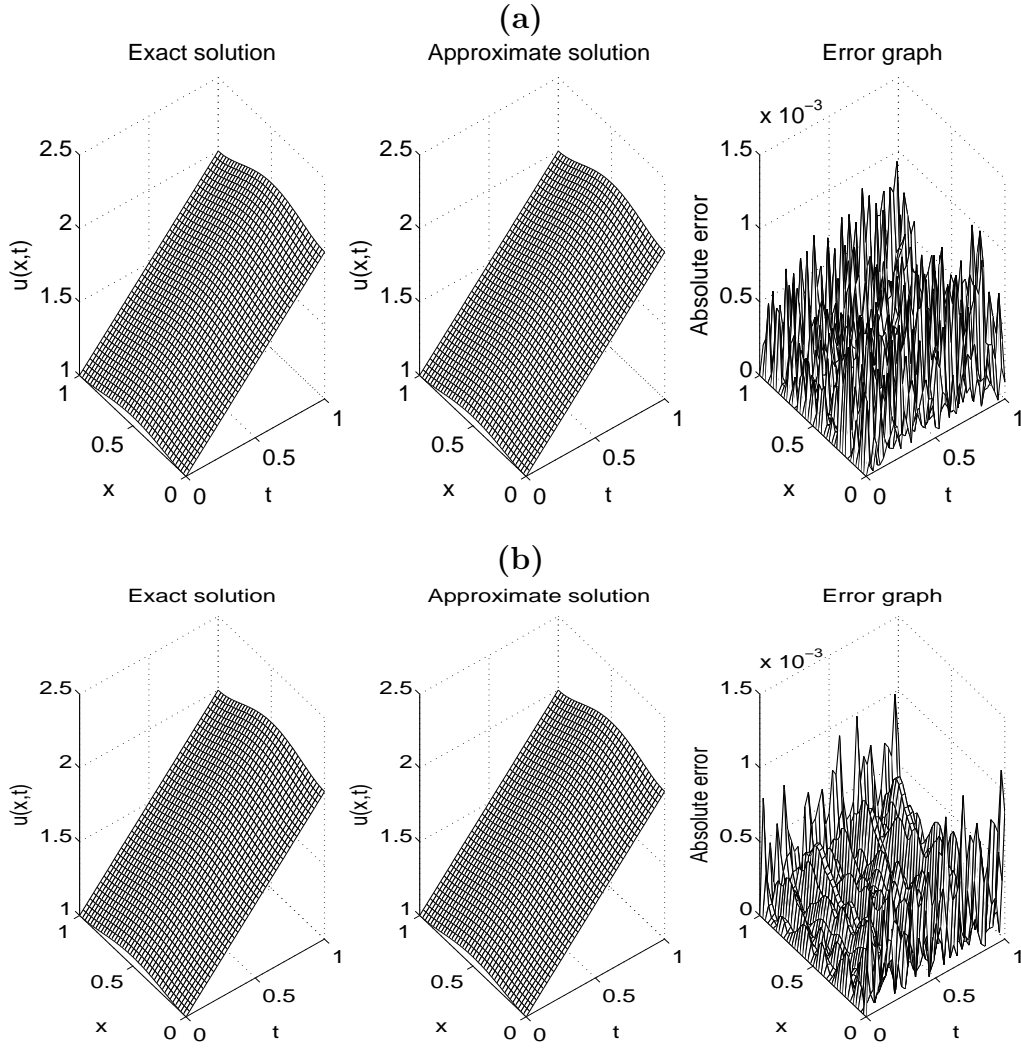
14

Figure 7: The exact and approximate solutions for the temperatures $u(x,t)$, for Example 1, with (a) $\beta_1 = \beta_2 = 0$ and (b) $\beta_1 = 10^{-9}$, $\beta_2 = 10^{-7}$, for $p = 0.01\%$ noise. The absolute error between them is also included.

5.2 Example 2

Consider the inverse problem (1)–(7) with the input data

$$\phi(x) = u(x,0) = 2 + \cos(\pi x), \tag{57}$$

$$\beta(t) = u(0.5,t) = 2e^{\frac{t^2}{1+t}}, \quad \psi(x) = u(x,1) = \sqrt{e}(2 + \cos(\pi x)), \quad \alpha = g(0.5) = 0. \tag{58}$$

As in Example 1, the conditions of Proposition 1 are satisfied and the unique solution of the inverse problem (1)–(7) is given by (10)–(12) which yield

$$f(t) = \frac{t(t+2)}{(t+1)^2}, \quad g(x) = \frac{\pi^2 \cos(\pi x)}{2 + \cos(\pi x)}, \tag{59}$$

$$u(x,t) = e^{\frac{t^2}{1+t}}\left(2 + \cos(\pi x)\right). \tag{60}$$

15

We take the initial guess as

$$f^0(t) = 0, \quad g^0(x) = \begin{cases} \frac{\pi^2}{3} - \frac{2\pi^2}{3}x, & 0 \le x \le 0.5, \\ \pi^2 - 2\pi^2 x, & 0.5 < x \le 1. \end{cases} \tag{61}$$

Analogous quantities and conclusions to Figures 3–6 and Table 2 of Example 1 are presented and obtained in Figures 8–11 and Table 3 of Example 2.
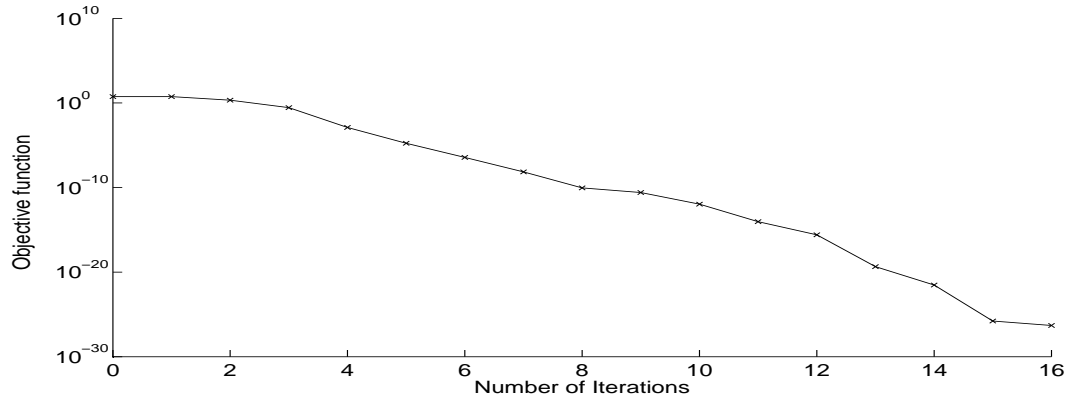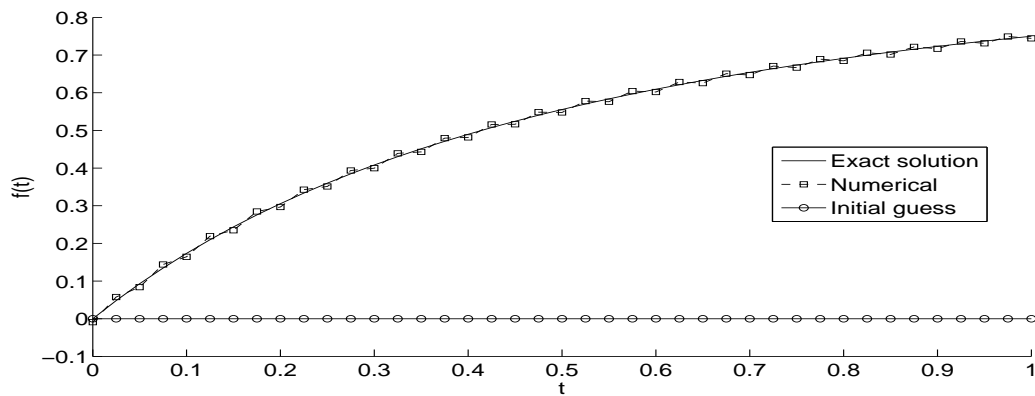

Figure 8: Objective function (49), for Example 2 with no noise and no regularization.
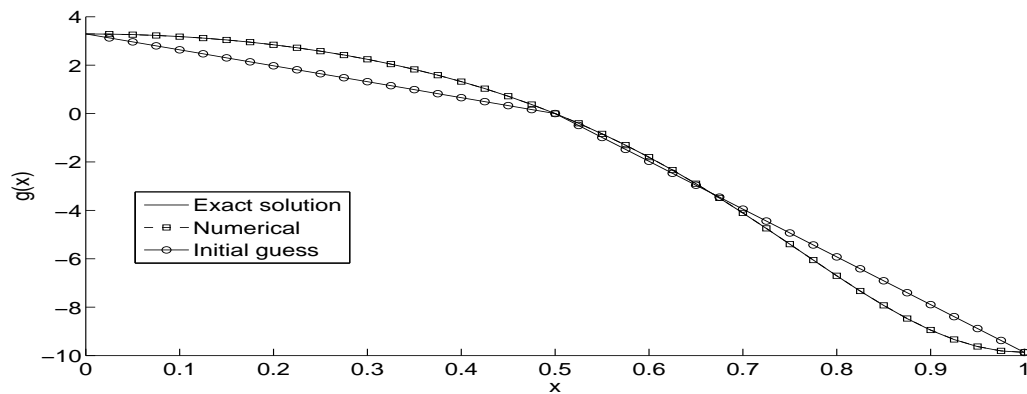
(a)

(b)

Figure 9: (a) Coefficient $f(t)$ and (b) coefficient $g(x)$, for Example 2 with no noise and no regularization.

Table 3: Number of iterations, number of function evaluations, value of the objective function (49) at final iteration, $rmse(f)$ and $rmse(g)$, and computational time, for Example 2.

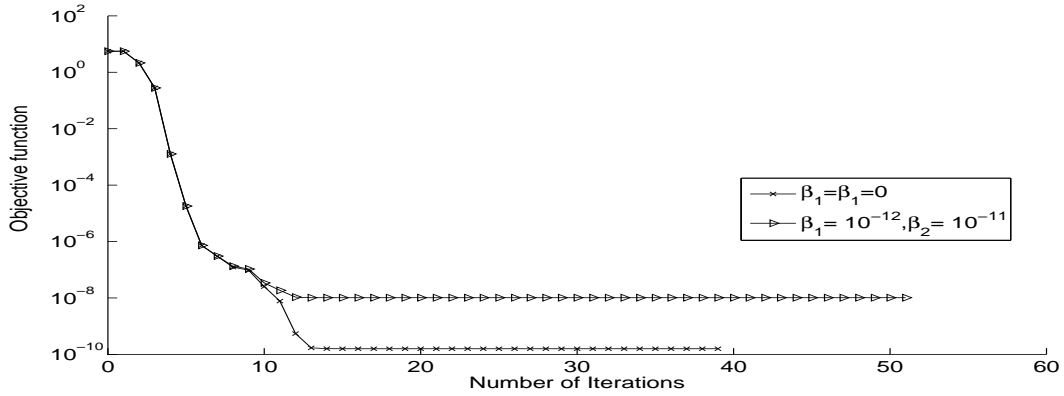| Numerical outputs	$p = 0$ $(\beta_1 = \beta_2 = 0)$	$p = 0.01\%$ $(\beta_1 = \beta_2 = 0)$	$p = 0.01\%$ $(\beta_1 = 10^{-12}, \beta_2 = 10^{-11})$
Number of iterations	16	39	52
Number of function evaluations	1411	3320	4316
Value of objective function (49) at final iteration	4.9E-27	1.5E-10	1.02E-8
$rmse(f)$	0.0077	0.1462	0.1084
$rmse(g)$	0.0025	1.2917	1.2847
Computational time (mins)	2	5	7

Figure 10: Objective function (49), for Example 2 with $p = 0.01\%$ noise, with and without regularization.

(a)

(b)

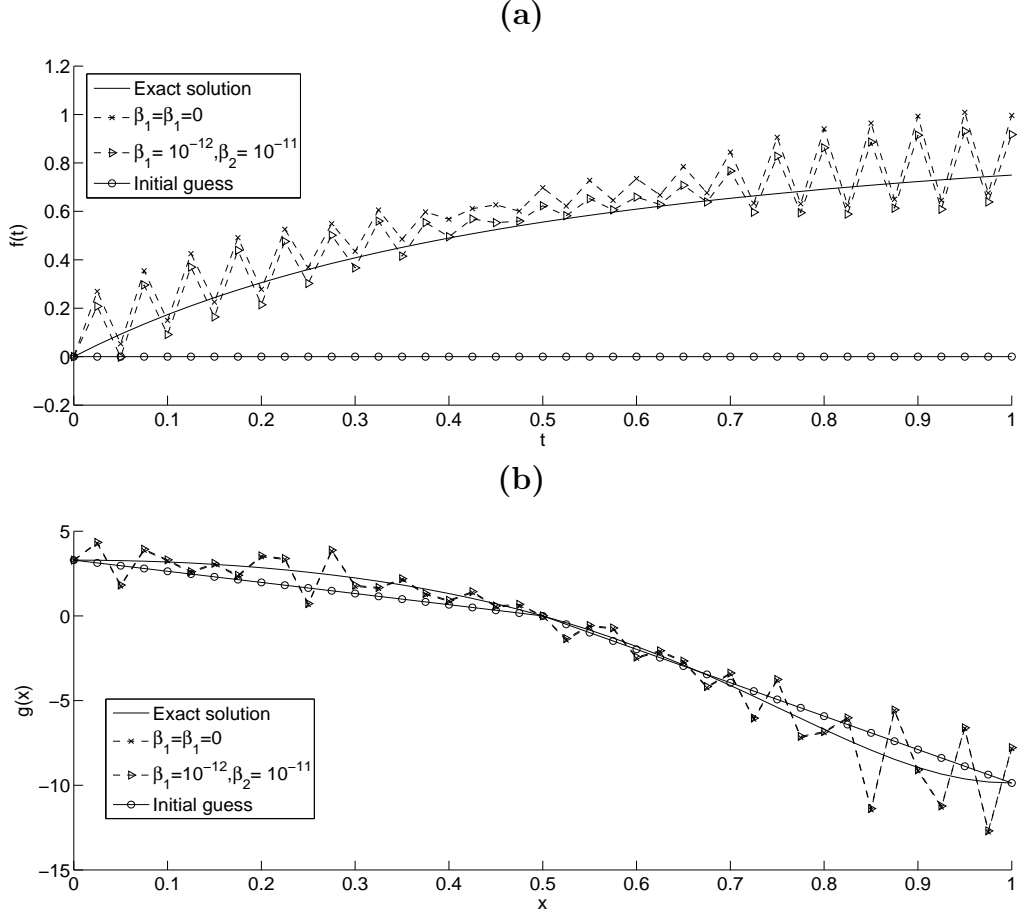
Figure 11: (a) Coefficient $f(t)$ and (b) coefficient $g(x)$, for Example 2 with $p = 0.01\%$ noise, with and without regularization.

5.3 Example 3

The previous examples possessed an analytical solution available for the triplet $(u(x,t), f(t), g(x))$. In this section, we investigate an example for which an analytical solution for $u(x,t)$ is not available. We take the initial condition (2) given by

$$u(x,0) = \phi(x) = \begin{cases} 1, & 0 \leq x < 1/4, \\ \frac{5}{4} - x, & 1/4 < x \leq 1/2, \\ x + \frac{1}{4}, & 1/2 < x \leq 3/4, \\ 1, & 3/4 < x \leq 1, \end{cases} \tag{62}$$

which represents a non-smooth function. In the absence of an analytical solution for $u(x,t)$ being available we generate the input data (4) and (5) numerically by solving first the direct problem given by (1)–(3) with $\phi(x)$ given by (62), and the known functions

$$f(t) = 1 + t, \quad g(x) = 1 + x, \tag{63}$$

using the FDM described in Section 3.

The numerical results for $\beta(t)$ and $\psi(x)$ in equations (4) and (5), respectivly, are shown in Figure 12, for various $M = N \in \{20, 40, 80\}$. From this figure, it can be seen that the numerical solution is convergent as the FDM mesh size decreases.

18

The example considered in this subsection violates the sufficient conditions of uniqueness of solution of Proposition 1 and (Savateev, 1995) and therefore, it is a severe test for our method of regularization.

In order to avoid committing an inverse crime the mesh that is used for numerically simulating the measured data (4) and (5) by solving the direct problem is taken to be more dense than the one used for the solution of the inverse problem, (Kaipio and Somersalo, 2007). Consequently, in the inverse problem we use the FDM with $M = N = 40$ and half of the data for β and ψ obtained from solving the direct problem with $M = N = 80$. We also take the initial guess as

$$f^0(t) = 1, \quad g^0(x) = 1. \tag{64}$$

The objective function (49) with no noise and no regularization, as a function of the number of iterations, is plotted in Figure 13. From this figure it can be seen that a rapid monotonic decreasing convergence to a low value of $O(10^{-28})$ is achieved in about 12 iterations.
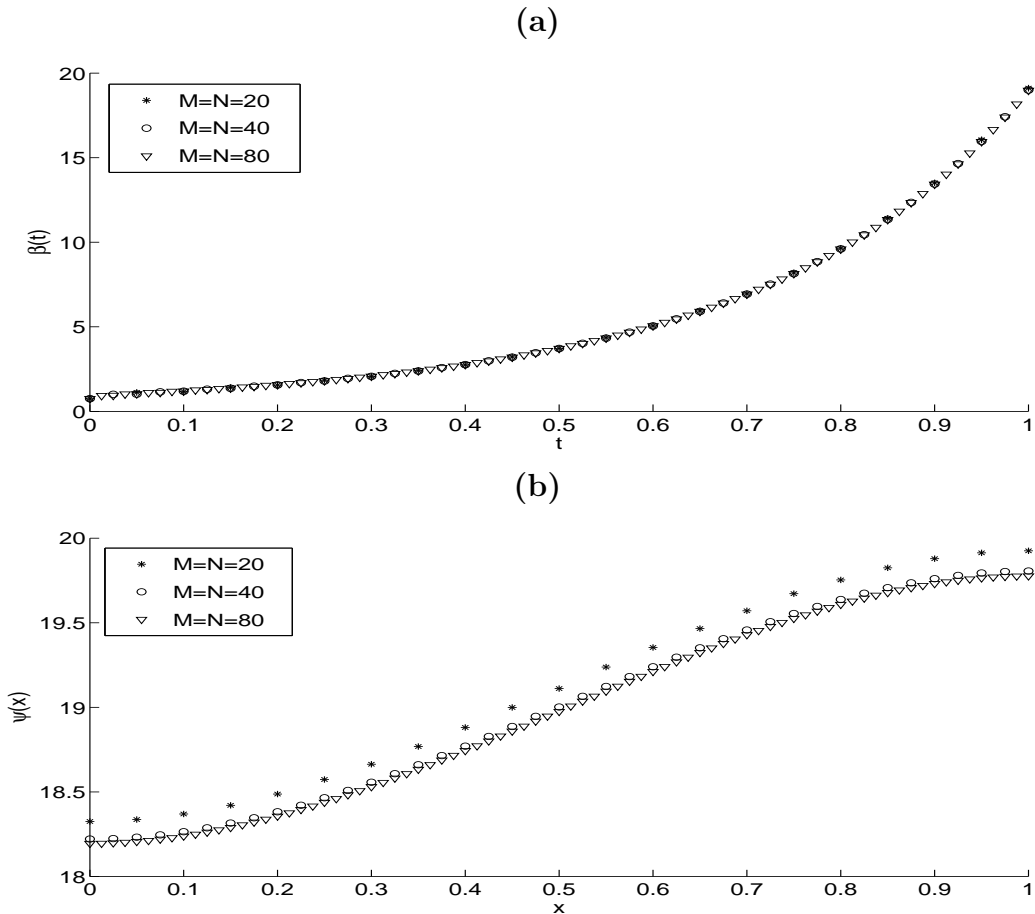
(a)

(b)

Figure 12: The numerically convergent solutions for (a) $\beta(t)$ and (b) $\psi(x)$, for Example 3 with various mesh sizes $M = N \in \{20, 40, 80\}$ for the direct problem.

Figure 14 shows the exact and numerical solution of the unknown coefficients $f(t)$ and $g(x)$, and one can see that stable and accurate solutions are obtained.
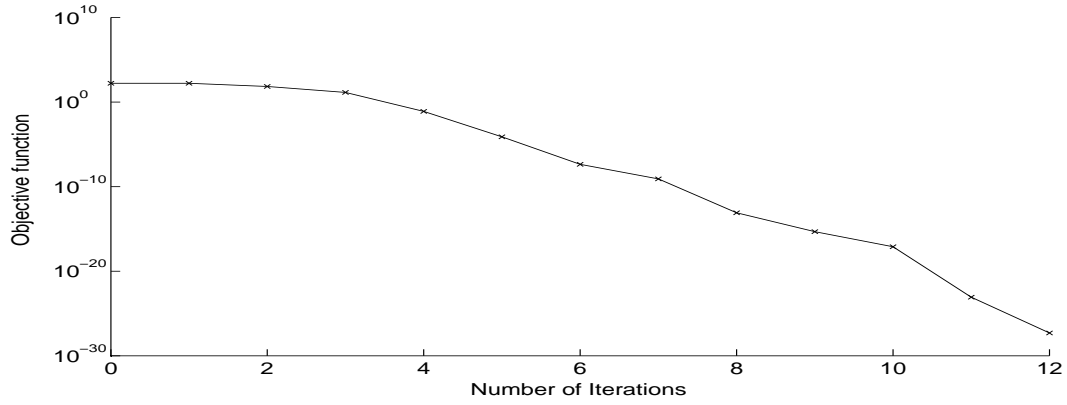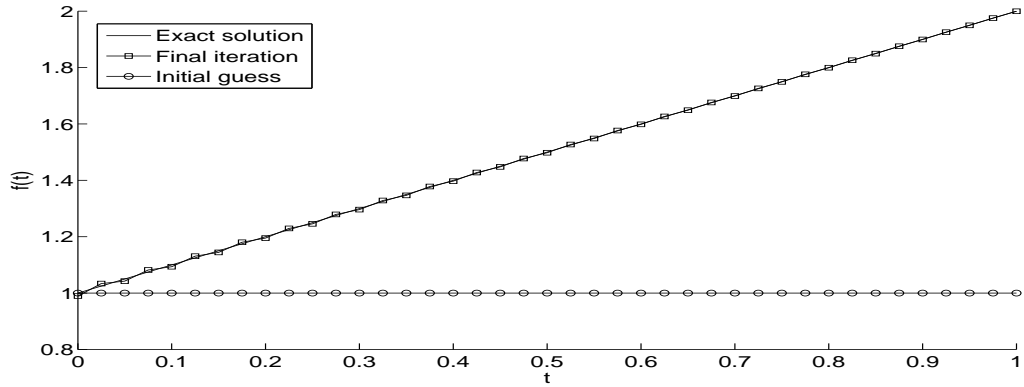
19

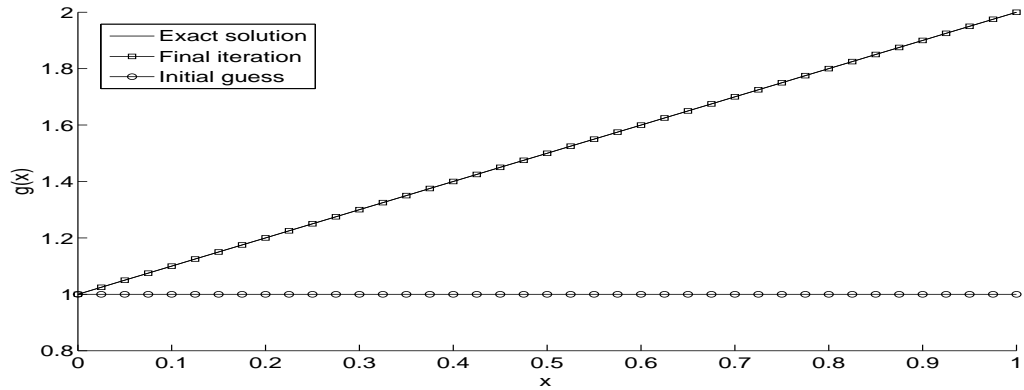Figure 13: Objective function (49), for Example 3 with no noise and no regularization.

Figure 14: (a) Coefficient $f(t)$ and (b) coefficient $g(x)$, for Example 3 with no noise and no regularization.

Next, we add $p \in \{0.01, 0.1, 1\}\%$ noise to the measured data (4) and (5). The numerical results without regularization have been found unstable and therefore they are not presented. The regularized objective function (49), as a function of the number of iterations, is shown in Figure 15. Figure 16 presents the graphs of the recovered functions. From this figure one can observe that stabilised solutions are obtained by employing regularization.

Finally, details about the number of iterations, the $rmse(f)$ and $rmse(g)$ in (54) and (55), respectively, and the computational time, are given in Table 4 for various values of the regularization parameters $\beta_1 = \beta_2$. For $p = 1\%$ noise and no regularization the computational time and the number of iterations increase drastically and the $rmse(f)$ and $rmse(g)$ become very large, which is expected due to the instability of the inverse and ill-posed problem. However, as previously obtained from Figure 16, it can be seen that accurate and stable numerical results are achieved if regularization is employed.
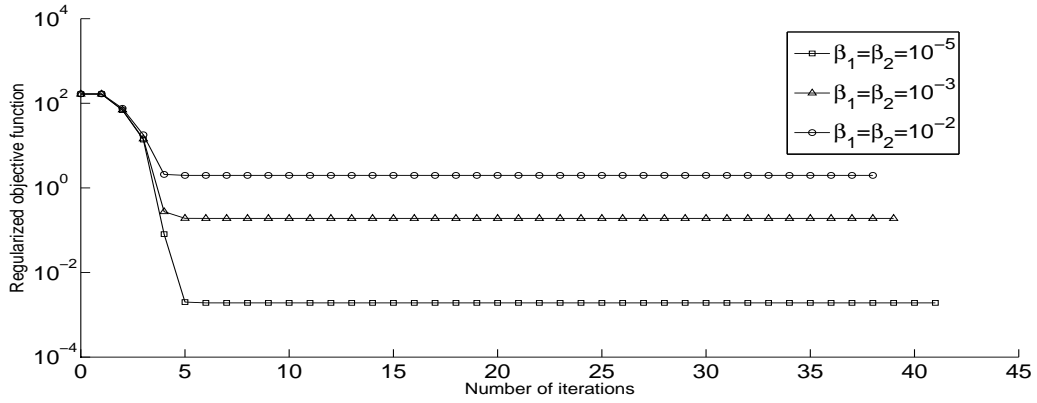

Figure 15: Objective function (49), for Example 3 with noise $p = 0.01\%$ ($-\square-$), $p = 0.1\%$ ($-\triangle-$) and $p = 1\%$ ($-\circ-$), with regularization.

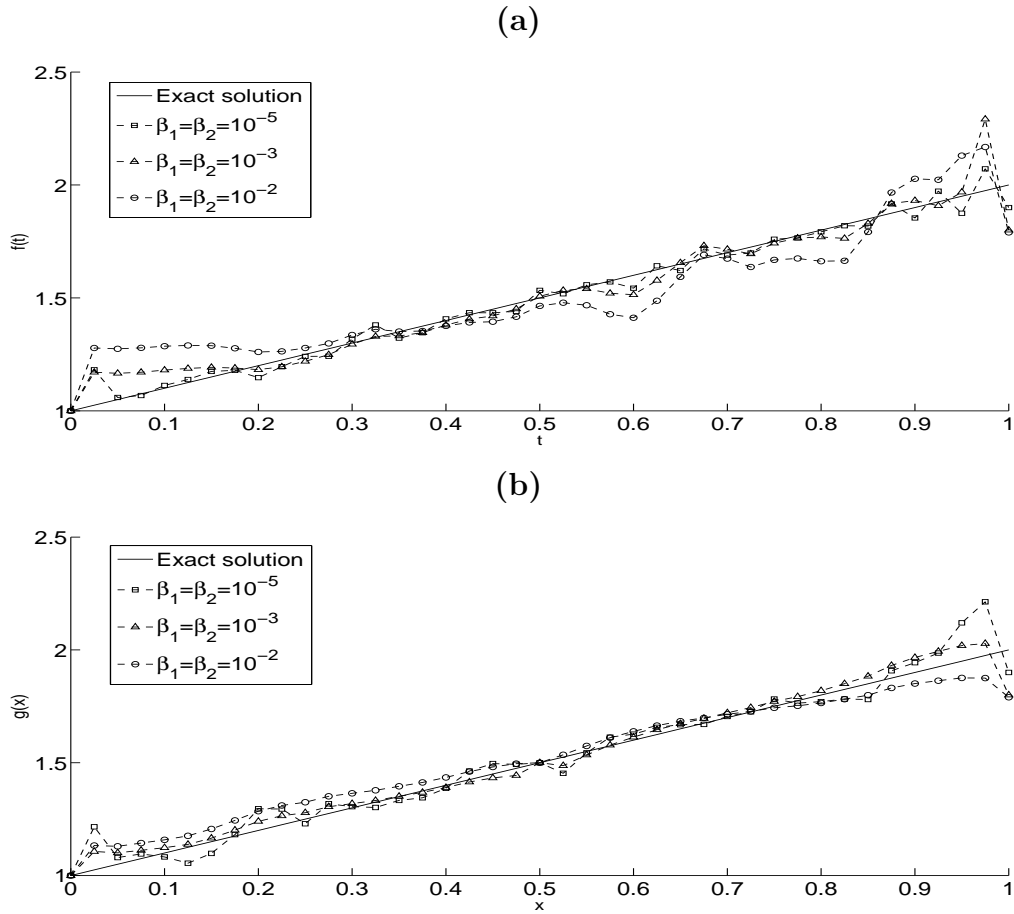Figure 16: (a) Coefficient $f(t)$ and (b) coefficient $g(x)$, for Example 3 with noise $p = 0.01\%$ $(-\square-)$, $p = 0.1\%$ $(-\triangle-)$ and $p = 1\%$ $(- \circ -)$, with regularization.

Table 4: Number of iterations, computational time, and *rmse* values for $p \in \{0.01, 0.1, 1\}\%$ noise, with and without regularization, for Example 3.

p	Regularization	$rmse(f)$	$rmse(g)$	Iter	Time
0.01%	$\beta_1 = \beta_2 = 0$	0.3373	0.5775	18	3 mins
	$\beta_1 = \beta_2 = 10^{-5}$	0.0406	0.0658	42	4 mins
	$\beta_1 = \beta_2 = 10^{-4}$	0.0525	0.0448	41	5 mins
	$\beta_1 = \beta_2 = 10^{-3}$	0.0613	0.0403	38	6 mins
	$\beta_1 = \beta_2 = 10^{-2}$	0.0899	0.0494	41	5 mins
	$\beta_1 = \beta_2 = 10^{-1}$	0.1831	0.1180	41	5 mins
0.1%	$\beta_1 = \beta_2 = 0$	3.3704	5.7759	47	8 mins
	$\beta_1 = \beta_2 = 10^{-5}$	0.2458	0.3619	47	8 mins
	$\beta_1 = \beta_2 = 10^{-4}$	0.1018	0.0895	39	6 mins
	$\beta_1 = \beta_2 = 10^{-3}$	0.0678	0.0335	39	6 mins
	$\beta_1 = \beta_2 = 10^{-2}$	0.0909	0.0466	50	9 mins
	$\beta_1 = \beta_2 = 10^{-1}$	0.1830	0.1197	50	9 mins
1%	$\beta_1 = \beta_2 = 0$	35.9469	53.9733	401	1 hour
	$\beta_1 = \beta_2 = 10^{-5}$	2.5250	3.5760	50	9 mins
	$\beta_1 = \beta_2 = 10^{-4}$	0.9086	0.7765	47	8 mins
	$\beta_1 = \beta_2 = 10^{-3}$	0.2720	0.1581	50	9 mins
	$\beta_1 = \beta_2 = 10^{-2}$	0.1139	0.0527	38	6 mins
	$\beta_1 = \beta_2 = 10^{-1}$	0.1820	0.1366	50	9 mins

6   Conclusions

This paper has presented the determination of an additive time and space-dependent perfusion coefficient from data measurements in the one-dimensional parabolic heat equation. The direct solver based on a Crank-Nicolson finite difference scheme was employed. The resulting inverse problem has been reformulated as a constrained regularized minimization problem which was solved using the MATLAB optimization toolbox routine *lsqnonlin*. The numerically obtained results are stable and accurate.

Future work will concern inversion of real physical temperature data (4) and (5) to reconstruct the additive time- and space-dependent perfusion coefficient in the context or bio-heat transfer, (Lesnic and Trucu, 2010) or the heat transfer coefficient in the context of fins used in condensers and evaporators, (Marin *et al.*, 2004).

Acknowledgments

References

[1] Belge, M., Kilmer, M. and Miller, E. (2002) Efficient determination of multiple regularization parameters in a generalized L-curve framework, *Inverse Problems*, **18**,

1161–1183.

[2] Coleman, T.F. and Li, Y. (1996) An interior trust region approach for nonlinear minimization subject to bounds, *SIAM Journal on Optimization*, **6**, 418–445.

[3] Deng, Z.C., Yang, L., Yu, J.N. and Luo, G.W. (2010) Identifying the radiative co-efficient of an evolutional type heat conduction equation by optimization method, *Journal of Mathematical Analysis and Applications*, **362**, 210–223.

[4] Deng, Z.C., Yu, J.N. and Yang, L. (2008) Optimization method for an evolutional type inverse heat conduction problem, *Journal of Physics A: Mathematical and Theoretical*, **41**, 035201, (20 pp).

[5] Fornasier, M., Naumova, V. and Pereverzyev, S.V. (2014) Parameter choice strategies for multipenalty regularization, *SIAM Journal on Numerical Analysis*, **52**, 1770–1794.

[6] Hazanee, A. and Lesnic, D. (2013) Reconstruction of an additive space- and time-dependent heat source, *European Journal of Computational Mechanics*, **22**, 304–329.

[7] Hao Dinh Nho, Thanh Phan Xuan, Lesnic, D. and Ivanchov, M. (2014) Determination of a source in the heat equation from integral observations, *Journal of Computational and Applied Mathematics*, **264**, 82–98.

[8] Kaipio, J. and Somersalo, E. (2007) Statistical inverse problems: discretization, model reduction and inverse crimes, *Journal of Computational and Applied Mathematics*, **198**, 493–504.

[9] Lewis, R.W., White, I.R. and Wood, W.L. (1978) A starting algorithm for the numerical simulation of two-phase flow problems, *International Journal for Numerical Methods in Engineering*, **12**, 319–329.

[10] Lesnic, D. and Trucu, D. (2010) The identification of blood perfusion coefficient in bio-heat transfer, *Inverse Problems, Design and Optimization Symposim (IPDO-2010)*, Joao Pessoa, Brazil, CD-ROM, pp. 277-284.

[11] Marin, L., Elliott, L., Heggs, P.J., Ingham, D.B., Lesnic, D. and Wen, X. (2004) Analysis of polygonal fins using the boundary element method, *Applied Thermal Engineering*, **24**, 1321–1339.

[12] Mathworks (2012) Documentation Optimization Toolbox-Least Squares (Model Fitting) Algorithms, available at www.mathworks.com/help/toolbox/optim/ug /brnoybu.html.

[13] Samarskii, A.A. and Vabishchevich, P.N. (2007) *Numerical Methods for Solving Inverse Problems of Mathematical Physics*, De Gruyter, Berlin.

[14] Savateev, E.G. (1995) On the problem of identification of a coefficient in a parabolic equation. *Siberian Mathematical Journal*, **36**, 177–185.

[15] Smith, G.D. (1985) *Numerical Solution of Partial Differential Equations: Finite Difference Methods*, Oxford Applied Mathematics and Computing Science Series, Third edition.

[16] Trucu, D., Ingham, D.B. and Lesnic, D. (2008) Inverse time-dependent perfusion coefficient identification, *Journal of Physics: Conference Series: 4th AIP Internatinal Conference and the 1st Congress of the IPIA*, **124**, 012050, (28 pages).

[17] Trucu, D. (2009) *Inverse Problems for Blood Perfusion Identification*, PhD Thesis, University of Leeds.

[18] Trucu, D., Ingham, D.B. and Lesnic, D. (2010) Space-dependent perfusion coefficient identification in the transient bio-heat equation *Journal of Engineering Mathematics*, **67**, 307–315.

[19] Trucu, D., Ingham, D.B. and Lesnic, D. (2011) Reconstruction of the space- and time-dependent blood perfusion coefficient in bio-heat transfer, *Heat Transfer Engineering,* **32**, 800–810.

[20] Wood, W.L. and Lewis, R.W. (1975) A comparison of time marching schemes for the transient heat conduction equation, *International Journal for Numerical Methods in Engineering*, **9**, 679–689.